# Temperature measurements and dissociation of shock-compressed liquid deuterium and hydrogen

N. C. Holmes, M. Ross, and W. J. Nellis

*University of California, Lawrence Livermore National Laboratory, Livermore, California 94550*

(Received 11 October 1994; revised manuscript received 30 May 1995)

Temperatures of shock compressed liquid deuterium and hydrogen up to 5200 K were measured at pressures up to 83 GPa (830 kbar). The measurements are in excellent agreement with earlier calculations to about 20 GPa and show evidence for dissociation above 20 GPa. At the highest measured temperatures and pressures current theories break down and a revised theory is proposed.

## I. INTRODUCTION

The high pressure equation of state, phase transitions, and metallization of hydrogen are topics of long-standing interest for scientific reasons and for applications to planetary physics and inertial confinement fusion. High pressure experiments are either static or dynamic, which encompass very different thermal regimes. Static methods achieved with the diamond-anvil cell are used to study the equation of state, optical properties, and phase transitions of solid hydrogen at room temperature or below. Dynamic compression achieved with shock or isentropic methods attains temperatures up to several thousand kelvin and complements static research. In some of our previous work on shock-compressed liquid hydrogen and deuterium we reported the results of Hugoniot (pressure-volume) measurements[1,2] and electrical conductivity.[3] At that time only theoretical Ross-Ree-Young (RRY) (Ref. 4) temperatures were available for shock-compressed hydrogen and deuterium. Over the past few years we have developed sophisticated optical methods for the measurement of temperature. These techniques were applied successfully to the dissociation of molecular nitrogen,[5,6] and the metallization of CsI (Ref. 7) and xenon.[8] The imaging systems used in those experiments are incompatible with the cryogenic techniques necessary for liquid $H_2$ and $D_2$ experiments. Our experimental method was recently redesigned to allow for greater sensitivity, accuracy, and convenience using fiber-optic coupling;[9] it has been applied to the shock melting of Fe.[10] The purpose of this paper is to present temperature measurements for single- and double-shocked liquid deuterium and hydrogen. Temperatures up to 5200 K have been measured at pressures up to 83 GPa (0.83 Mbar) in the fluid phase. The results of single-shock experiments to 20 GPa and 4600 K are in excellent agreement with earlier calculations.[4] These temperatures were used to derive an effective electron band gap in hydrogen from the electrical conductivity measurements.[3] Our temperature measurements at substantially higher double-shock pressures indicate a considerable amount of molecular dissociation is present. As a result, the earlier theory was found to be inadequate and has been revised. Thus, the high temperatures achieved in these experiments provide an important constraint to the development of theoretical models.

Theoretical studies have had a long history of predicting the metallization pressure of hydrogen beginning with Wigner and Huntington.[11-13] Current estimates of the pressure needed to form a monatomic solid at 0 K are in the 300–400 GPa range, although some considerable uncertainty remains because of uncertainties in the crystal structure, molecular orientation, and intramolecular zero-point motion.[14-16] A solid-solid phase transition was originally reported to terminate in a critical point at 150 GPa and 140 K.[17,18] Recently, phase transitions in $D_2$ have been reported to meet at a triple point at 153 GPa and 128 K, and above this point a phase line persists to 186 GPa and 210 K.[19] While the origins of these phase transitions remain unresolved, some speculation rests on the possibility that they might be the result of a molecular insulator to molecular metal transition. Measurements in the solid are limited to pressures below 250 GPa and the states appear to be molecular. The status of research on the molecular solid state has recently been reviewed.[20]

From the standpoint of applications, the major interest in the equation of state, phase transitions, and metallization of hydrogen is the fluid phase at high pressures and temperatures. The fluid is expected to become metallic near the same pressure as the solid but to occur in a continuous manner starting with dissociation at a lower pressure. In the case of shock-compressed liquid nitrogen the initial stages of a continuous dissociative transition have been observed.[5,6] Until now, because of the absence of shock temperature measurements, a similar effect has not been observed in hydrogen. The results of this study show that at the conditions of our experiment, hydrogen is undergoing a similar dissociative transition which is the precursor to the fully dissociated liquid metallic state.

The present paper is organized in five sections: In Sec. II we describe the experimental method and present the results; in Sec. III we develop a theoretical model which is necessary for analyzing the experimental results and provides a means of generating numerical data for applications. Section IV reviews the calculation of single- and double-shock Hugoniots. In Sec. V, we discuss some of the ramifications of our results.

## II. EXPERIMENTAL METHOD

Strong shocks were generated in the liquid samples by impact of projectiles driven by a two-stage light-gas gun.[21] The deuterium or hydrogen samples were condensed from pure gas in a cavity cooled to 20 K by an outer cooling jacket filled with liquid $H_2$ using sample preparation and cryogenic methods developed by Nellis *et al.*,[1] shown schematically in Fig. 1. The sample cavity was a cylinder, 20 mm in diameter and 1.5 mm thick. On the side impacted by the projectile
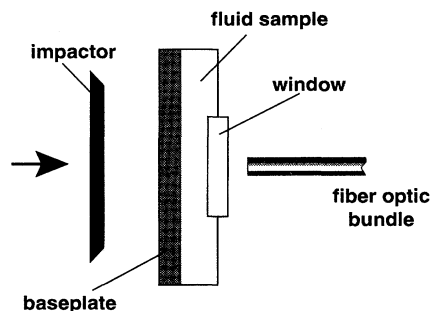
FIG. 1. Schematic of the sample holder, not to scale. The impactor arrives from the left and generates a shock wave in the baseplate at impact. When the shock enters the fluid sample, it becomes highly luminous. The fiber optic bundle collects the emitted light after passing through the window. The shock in the sample is reflected by the higher shock impedance window to higher pressures, temperatures, and densities.

(front) the cylinder was bounded by a 2 mm thick plate of aluminum (1100 alloy), and the rear was formed by a synthetic sapphire ($Al_2O_3$) or LiF window 3 mm thick. The window was used to allow optical access for the temperature measurements described below. The impactor velocity was measured by flash radiography[22] to an accuracy of 0.1%. The measured impactor velocity was used to determine the shock pressure by impedance matching.[1] The initial sample temperatures and densities were taken as nominal values measured in previous experiments.[1] These values are insensitive to barometric variations. A Pt resistance thermometer was used to monitor the temperature (to ensure that liquid $H_2$ or $D_2$ was condensing) and a capacitance manometer was used to measure the sample cavity pressure during the process of condensing the liquid samples up to the time just prior to shock compression. The liquid samples were pressurized with their own gas to a pressure at least 100 torr higher than saturation pressure to obtain a quiescent sample free of bubbles.

Shock temperatures were determined by analysis of the light emitted from the shocked samples. The sample geometry was chosen to allow us to observe both single- and multiple-shocked samples in the same experiment. The rise time of the light emission from the sample indicates that they become optically thick within a few ns, short compared to the roughly 100 ns shock transit time. When the first shock in the sample reaches the window, which is of higher shock impedance than the fluid samples, the shock is reflected; the sample is thus reshocked to a new state of higher pressure and density. The shock reverberates between the baseplate and window, eventually reaching a constant state. The increase in temperature with each reverberation leads to an increase in intensity of the light emitted from the sample. For some combinations of first and final shock temperatures, that increase is beyond the dynamic range of our recording system. That is, we can choose to measure the temperature of the first few shocks or the final state, but not both. The shock impedance match process is illustrated in Fig. 2, and described in the caption. A theoretical model is *required* to obtain the pressure and volumes at which the second-shock temperatures were measured.
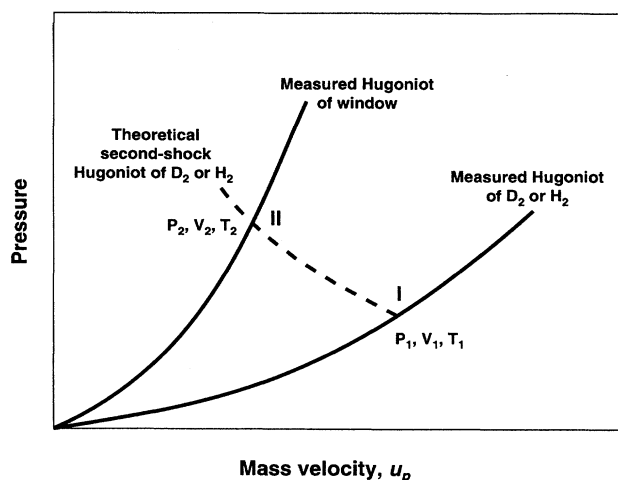


**Mass velocity, $u_p$**

FIG. 2. Shock impedance-match plot for the first and second shock states in $D_2$ and $H_2$ (points I and II) obtained in the configuration of Fig. 1. The second shock is also termed the reshock, reflected shock, or double shock. Shock pressure $P$ and mass velocity $u_p$ [see Eq. (16)] are continuous across the interfaces between materials. Thus, the loci of possible shock states (Hugoniot curves) for two adjacent materials will intersect when plotted in the $P$-$u_p$ plane. The first-shock state (I) is obtained from the measured impactor velocity and the previously measured Hugoniot equations of state of the Ta impactor, Al baseplate, and liquid $D_2$ or $H_2$ sample. The second shock state (II) is found by the intersection of the theoretically calculated Hugoniot of $D_2$ or $H_2$ using state I as the starting state (dashed curve), and the previously measured equation of state of the window material. The model is adjusted to agree with all previous measurements of the equations of state of $D_2$ or $H_2$ and the measured first- and second-shock temperatures. When these temperatures agree, the model gives the values of pressure and density of the second-shock state.

Here we will report only the results of the first-shock and the reshock (or second-shock) states. We performed reshock experiments using two different window materials of differing shock impedances, $z$-cut synthetic sapphire (which has its $c$ axis parallel to the direction of shock propagation), and LiF. For a given first shock, each window will produce a reshock of different pressure and temperature. This provides an excellent test of the models discussed below for states off the principal Hugoniot. The shocked states in the samples were found using impedance matching.[23,24] For the first-shock state, we can determine the pressure, density, and internal energy using the impactor velocity and initial densities of the sample, impactor, and baseplate. We make use of the known equations of state for the Ta impactor,[25,26] the Al baseplate,[1,25] and the measured equation of state (EOS) of $D_2$ or $H_2$.[1] In a similar fashion, the reshock states were found using the known first-shock state, the Hugoniot of synthetic sapphire[27,28] or LiF,[27] and the theoretical equations of state of $D_2$ and $H_2$ adjusted to agree with the measured temperatures, as described in Secs. III and IV.

Shock temperatures were measured optically using a six-channel fiber-optic-coupled optical pyrometer.[9] For these experiments, a seven-fiber bundle was positioned 1 mm away from the window to minimize thermal loading of the sample cavity, and to preclude possible damage to the bundle from
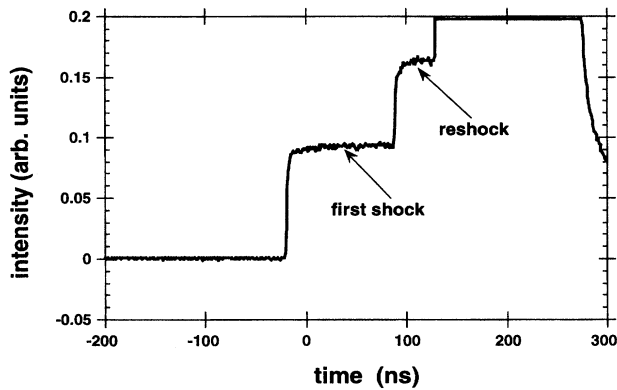
FIG. 3. Photomultiplier output vs time at 598 nm center wavelength in experiment $D_2$ No. 1 showing the first- and second-shock intensities. The constant output (flat regions) indicates that the temperature is constant during shock transit, and the rapid rise times arise from the short time required for the $D_2$ to become optically thick. The onset of the fourth shock in $D_2$ (the second shock in the sapphire window) at about 120 ns causes an increase in intensity that is beyond the range of the recording system. The zero time is arbitrary.

the low temperature. We mounted the bundle within a thin steel ring connected to the target by thin steel spokes. The seventh fiber was used to check for any deposition of ices on the outer window surface. We diamond-turned the inside surface of the Al baseplate to a mirror finish. A light source was focused onto the seventh (center) fiber outside the target chamber. The light emitted from the fiber reflected off the Al baseplate surface and some of the reflected light was collected by the other fibers in the bundle. We measured the amount of light collected before the target cooled, and again just before the experiment when the sample cavity was filled. Since the signal was the same in both cases, we know that the optical system was free of any obscuring deposits on the window.

Each of remaining six fibers was coupled to six fast photomultipliers through narrow-band [20 nm full width at half maximum (FWHM)] interference filters centered at six wavelengths between 340 and 700 nm, with additional calibrated neutral density filters added as appropriate. Filter values were chosen to keep the signals well within the linear response range of the photomultiplier circuits. The outputs of the photomultipliers were recorded on 1-GHz bandwidth transient digitizers, with a 1-GHz sample rate. A typical record (experiment $D_2$ No. 1) is reproduced in Fig. 3 for $D_2$ shocked to 22 GPa, and reshocked to 83 GPa. It shows that the signal is constant during shock transit and reshock, a consequence of the steady shock waves produced by the impact process, and that the shocked $D_2$ is optically thick as indicated by the fast rise times.

We used calibration signals recorded with a 3200-K tungsten calibration lamp to find the radiance (W/m²/sr) at each of the measured wavelengths during the entire shock experiment. The radiance of this lamp, which we use as a secondary standard, was calibrated by comparison with a NIST-traceable bolometric calibration of a standard W ribbon lamp which we use as our primary standard lamp.[9] The radiance
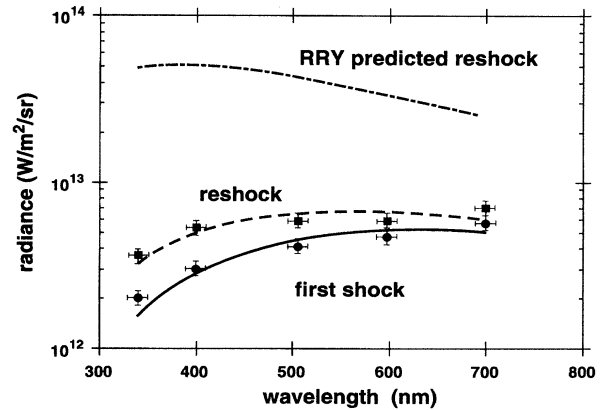


FIG. 4. Results of nonlinear least-squares fits to the radiance data for experiment $D_2$ No. 3. Error bars in radiance are estimated from the uncertainties in calibration as well as the scatter of the fit, while those in the wavelength direction indicate the spectral bandwidth of the channels. The solid circles are data from the first shock, while solid squares indicate measurements of reshock intensities. Also plotted are predicted intensities for a reshock temperature calculated with the RRY model (Ref. 4) for the same first-shock pressure and $\epsilon = 0.7$ (see Fig. 8). The lower radiance we observe, as well as the shift of the peak of the grey-body spectrum, substantiates our observations of considerably lower reshock temperatures than those predicted with RRY.

values in the experiments were corrected for the reflectivity of the $D_2$-window interface. The corrected values of the six channels were fit to a grey-body Planck spectrum

$$I(\lambda) = \epsilon \frac{2\pi hc^2}{\lambda^5} \left( \exp \frac{hc}{\lambda kT} - 1 \right)^{-1}, \qquad (1)$$

where $I$ is the radiance, $\epsilon$ is the emissivity, $\lambda$ is the wavelength, $T$ the (kelvin) temperature, $h$ is Planck's constant, $c$ the velocity of light, and $k$ is Boltzmann's constant. In our analysis, we assumed $\epsilon$ did not depend on wavelength. While it is tempting to use the Wien displacement relation for the peak of the grey-body spectrum (i.e., $\lambda_{peak} = 3000/T$) to determine the temperature, this requires a large number of channels to accurately determine the peak. It is easy to show using Eq. (1) that the fit is more sensitive if the spectrum is sampled on the short wavelength side of the peak. Furthermore, the photomultipliers we use have an S-20 response, and are not very sensitive in the infrared where the peaks of many of the first-shock spectra lie. These factors motivated our choice of spectral channels. We used a nonlinear least-squares method to find the values of $\epsilon$ and $T$. Error estimates are calculated using the covariance matrix of the fitted data,[29] and are typically $\approx 100-200$ K, and 0.15 in $\epsilon$. These arise from the roughly 10% uncertainties in the measured intensities, as indicated by the error bars in the figure. For shot $D_2$ No. 3, Fig. 4 shows the fit for the first- and second-shock records. In the figure, we have also plotted the expected emission data for a reshock temperature calculated using the RRY model,[4] which assumed that no internal energy is absorbed in dissociation. The temperatures predicted by that

TABLE I. Summary of shock temperature experimental materials and impact velocities (km/s). In all experiments, the baseplate was 1100 aluminum, nominal sample densities are 0.171 g/cm$^3$ for D$_2$, 0.071 g/cm$^3$ for H$_2$, and the Al$_2$O$_3$ ($\rho = 3.98$ g/cm$^3$) and LiF ($\rho = 2.64$ g/cm$^3$) windows were single crystals. The impactor materials were 1100 aluminum (Al) or tantalum (Ta).

| Shot name | Sample material | Impactor material | Impactor velocity | Window material |
|---|---|---|---|---|
| D$_2$ No. 1 | D$_2$ | Ta | 7.006 | Al$_2$O$_3$ |
| D$_2$ No. 2 | D$_2$ | Ta | 4.903 | Al$_2$O$_3$ |
| D$_2$ No. 3 | D$_2$ | Ta | 6.646 | Al$_2$O$_3$ |
| D$_2$ No. 4 | D$_2$ | Ta | 5.941 | Al$_2$O$_3$ |
| D$_2$ No. 5 | D$_2$ | Al | 7.135 | LiF |
| H$_2$ No. 1 | H$_2$ | Ta | 7.220 | Al$_2$O$_3$ |

TABLE II. Pressures, temperatures, and emissivities for single shock ($P_1, T_1, \epsilon_1$) and reshock ($P_2, T_2, \epsilon_2$) temperature measurements on liquid D$_2$ and H$_2$. Pressures are expressed in GPa (1 GPa $= 10^4$ bars), and temperatures are in K, with nominal experimental uncertainties of 100–200 K. For experiments D$_2$ No. 5 and H$_2$ No. 1, reshock intensities were not recorded as they were beyond the intensity range of the data recording system.

| Name | $P_1$ | $T_1$ | $\epsilon_1$ | $P_2$ | $T_2$ | $\epsilon_2$ |
|---|---|---|---|---|---|---|
| D$_2$ No. 1 | 22.6 | 4660 | 0.9 | 86.5 | 5210 | 0.9 |
| D$_2$ No. 2 | 12.0 | 2820 | 0.33 | 52.5 | 3910 | 0.9 |
| D$_2$ No. 3 | 20.6 | 4430 | 0.76 | 81.0 | 5030 | 0.64 |
| D$_2$ No. 4 | 16.9 | 3800 | 0.6 | 70.0 | 4260 | 0.6 |
| D$_2$ No. 5 | 23.4 | 4530 | 0.9 | 77.1 | 4960 | 0.9 |
| H$_2$ No. 1 | 11.3 | 3360 | 0.9 | – | – | – |

model are demonstrated in the figure by the substantially higher value of radiance and the shift in peak position relative to our measurements.

To ensure that the measured double-shock temperatures are accurate, four checks were made. The concern here is caused by the fact that the optical emission we record from the second shock state traverses a window through which a shock wave is traveling. Shock compression of the window might change its optical properties. Thus, it is important that shock-induced changes in optical properties of the window have little or no effect on the radiation emitted from the hydrogen sample. The checks were as follows. First, the time dependence of the first- and second-shock optical signals are as expected: sharp rises in intensity with nearly instrumental resolution followed by a constant amplitude signal (see Fig. 3). These occur after shock arrival in the sample from the Al baseplate and after the first shock reflects off the window. Second, two experiments were performed with Al$_2$O$_3$ windows to demonstrate that the measurements are reproducible. The results for D$_2$ No. 1 and D$_2$ No. 3 show that this is the case; see Table II. Third, the window was changed to LiF in D$_2$ No. 5 to show that the results are not dependent on window material. A double-shock temperature with a LiF window was measured as predicted from a model based on experiments with Al$_2$O$_3$ windows. In fact, the temperatures measured with the two windows are quite close to each other because of the nature of the shock reflection process in hydrogen. Thus, the use of two different window materials successfully tested their optical properties under shock compression. Fourth, the optical intensity of Al$_2$O$_3$ shocked to 85 GPa (without the presence of liquid hydrogen), essentially the same as our maximum pressure, is much lower in magnitude and shows a totally different slow rise time than our measured optical intensities.[30] In other words, the known optical emissions from the Al$_2$O$_3$ window are too weak to contribute to our measured optical intensities from which we determine our temperatures. Because of all of these reasons, we are measuring the true optical intensities from double-shocked hydrogen.

In Table I we list the materials and impact velocities for each of the experiments, and in Table II we list the first shock and reshock temperatures and emissivities; these are compared to the calculations of the present model as described below, and summarized in Table III. We used both liquid D$_2$ and liquid H$_2$ samples to check for consistency of the model; H$_2$ has less than half of the initial density of D$_2$, and thus H$_2$ reaches states of relatively lower pressure and temperature than D$_2$ using the same impact conditions. We also attempted to measure the final "ring-up" temperatures of D$_2$ at 110 GPa final pressure (after the reverberations between the Al baseplate and Al$_2$O$_3$ window reached the constant state) using both sapphire and LiF windows. Those attempts failed, evidently due to the loss of transparency of the windows due to multiple shocks. The optical properties of the windows changed when reshocked (corresponding to the fourth shock in D$_2$) at pressures of roughly 80–100 GPa; this was identified by hydrodynamic simulations of the experiments.

As noted above, we need to use a theoretical equation of state for hydrogen to perform impedance match calculations for shocks which reflect from the window. For this purpose, the equation of state model described in the next section was developed to fit all existing shock data for liquid hydrogen and deuterium. The model was constrained to fit the soft-sphere fluid theory in the low-density molecular limit and extend in a continuous fashion to the free-electron gas at high density. It was also required to reduce to the generally accepted theoretical models of solid hydrogen at low temperature and metalliclike density. The second-shock pressures and densities shown for the present model in Table III were obtained by impedance matching the $P$-$u_p$ curves predicted by the model against the $P$-$u_p$ curves for the window materials.

### III. THEORETICAL MODEL

The objective of the present theoretical work is to provide a computationally simple model which (i) includes molecular dissociation, (ii) accurately reproduces all measured shock temperatures and Hugoniots of liquid D$_2$ and H$_2$, and (iii) yields the pressures and volumes at which our second-shock temperatures were measured. For those thermodynamic states in which dissociation is negligible, the equation of state of molecular hydrogen can be accurately determined by the use of pairwise additive forces obtained from fitting experimental static and shock data.[4,31] At very high densities, the equation of state of completely dissociated hydrogen can be approximated as a nearly-free-electron metal. However,

TABLE III. Experimental and calculated shock temperatures and densities for single- and double-shocked $D_2$, and for a single shock in $H_2$. The results of calculations using the present model (see text) are listed along with the calculated fraction of $D_2$ or $H_2$ dissociated. The reshock states were calculated using shock impedance matching with the known equation of state of synthetic sapphire (see Fig. 2). Volumes are expressed in $cm^3/mol$, pressures in GPa, temperatures in K. The experimental uncertainty of the temperature measurements is 100–200 K. $x$ is the fraction of $D_2$ or $H_2$ dissociated.

| | | First shock | | | | Second shock | | | |
| | | $V_1$ | $P_1$ | $T_1$ | $x_1$ | $V_2$ | $P_2$ | $T_2$ | $x_2$ |
| --- | --- | --- | --- | --- | --- | --- | --- | --- | --- |
| $D_2$ No. 1 | experiment | 7.02 | 22.6 | 4660 | a | — | — | 5210 | — |
| | model | 7.02 | 20.5 | 4411 | 0.0198 | 3.65 | 82.8 | 5162 | 0.22 |
| $D_2$ No. 2 | experiment | 7.98 | 12.0 | 2820 | — | — | — | 3910 | — |
| | model | 7.98 | 13.1 | 2867 | 0.0006 | 4.51 | 52.5 | 4008 | 0.05 |
| $D_2$ No. 3 | experiment | 7.15 | 20.6 | 4430 | — | — | — | 5030 | — |
| | model | 7.15 | 19.4 | 4213 | 0.0145 | 3.76 | 78.2 | 5034 | 0.19 |
| $D_2$ No. 4 | experiment | 7.44 | 16.9 | 3800 | — | — | — | 4260 | — |
| | model | 7.44 | 17.1 | 3749 | 0.0062 | 4.00 | 68.8 | 4701 | 0.13 |
| $D_2$ No. 5 | experiment | 6.92 | 23.4 | 4530 | — | — | — | 4960 | — |
| | model | 6.92 | 21.3 | 4560 | 0.025 | 3.85 | 74.2 | 5095 | 0.18 |
| $H_2$ No. 1 | experiment | 8.9 | 11.3 | 3360 | — | — | — | b | — |
| | model | 8.9 | 11.2 | 3381 | 0.001 | — | — | — | — |

[a]The experiment does not determine $V_2$, $P_2$; nor does it measure the dissociation fraction $x$, and this is indicated for all experiments by dashes. These values are determined by the model.

[b]Reshock temperature data were not recorded for experiment $H_2$ No. 1 due to increase in brightness beyond the instrumental range. Thus, reshock states were not calculated.

the problem arises in the intermediate region of partial dissociation where the interatomic forces are unknown. Previous work[4,31] using pairwise potentials for the atom-atom and atom-molecule interactions have been found to predict second-shock temperatures which are too high by about 40% (see Figs. 3 and 8). These results indicate that the effective interactions in the dissociated mixture are much softer and a more realistic treatment of the interactions are necessary. Recently, calculations have been reported for partially dissociating dense hydrogen using the *ab initio* quantum Monte Carlo (QMC) method.[32] This method is in principle exact, but computationally intensive, requiring thousands of hours of CRAY-YMP time for calculating the large number of data points needed to accurately characterize an equation of state. QMC calculations indicate that the structure of the dissociating mixture is a complicated arrangement of molecules and strings of atoms. These QMC computations illustrate the complexity of first-principles calculations on dense hydrogen at high densities and temperatures.

### A. Ideal mixing model

In order to reduce the complexity of the problem to a level appropriate for a simple model, we assume that the thermodynamic properties of the dissociating fluid can be expressed, using the ideal mixing model, as an average of the pure molecular and monatomic hydrogen equations of state. This mixing model is described in detail by Guggenheim.[33] Our *ansatz* builds in the correct limiting behavior for the low-density molecular fluid and high-density monatomic

fluid and interpolates smoothly between. This model does not explicitly include atom-molecule interactions. Our phenomenological model is appropriate for a mixture which is primarily molecular with a modest amount of dissociated molecules ($\leq 20\%$). We write the Helmholtz free energy for a system of $N$ molecules as

$$F(V,T,x) = (1-x)F_{H_2}(V,T,x=0) + xF_{H\text{-}H}(V,T,x=1)$$
$$- TS_{mix} - (1-x)D^0, \qquad (2)$$

where $x$ is the fraction of dissociated molecules. It is determined by minimizing $F$. $F_{H_2}$ and $F_{H-H}$ are, respectively, the free energies of the pure molecular and monatomic components per two atoms and $V$ is the molar volume per molecule or two atoms. $S_{mix}$ is the entropy of mixing $H_2$ and H:[33]

$$S_{mix} = -k\left[(1-x)\ln\left(\frac{1-x}{1+x}\right) + 2x\ln\left(\frac{2x}{1+x}\right)\right]. \qquad (3)$$

$D^0 = -4.735$ eV is the diatomic bond well depth, or the value of the dissociation energy, omitting the vibron energy. The superscript 0 is used here to denote the use of isolated gas values. Ideal mixing gives no change in the energy and hence no contribution to phase separation other than $TS_{mix}$. Typically, mixing energies have small absolute values when compared to $F_{H_2}$ and $F_{H-H}$ and make contributions of only a few percent or less to the total pressure and energy.

## B. Molecular fluid

The method for calculating $F_{H_2}$ has been described in detail elsewhere.[4] It is briefly summarized below. We write $F_{H_2}$ as

$$F_{H_2} = F^0_{H_2} + F^0_{H_2 int} + F_{H_2 conf}, \tag{4}$$

where $F^0_{H_2}$ is the translational free energy and $F^0_{H_2 int}$ is the contribution from the rotational and vibrational degrees of freedom. Ideal gas values are assumed, and electronic excitation is neglected. The term $F_{H_2 conf}$, the configurational free energy, is calculated from soft-sphere fluid variational theory:

$$F_{H_2 conf} = F_{HS}(\eta) + F(\eta) NkT$$
$$+ (\rho N/2) \int d^3r \phi(r) g_{HS}(r,\eta), \tag{5}$$

where $\eta = \pi d^3/6$, $F_{HS}(\eta)$ is the hard-sphere excess free energy, and $g_{HS}(r,\eta)$ is the hard-sphere radial distribution function. $d$, the hard-sphere diameter of the reference system, is the variational parameter used to minimize $F_{H_2 conf}$. The factor $F(\eta) = -(\eta^4/2 + \eta^2 + \eta/2)$ added to the hard-sphere free energy makes the reference system equivalent to a softer inverse-12 power repulsion with the result that thermodynamic data computed from Eq. (4) agree with computer simulation data for a broad class of potentials including those in this study. $\phi(r)$ is the $H_2$-$H_2$ pair potential. It had previously been obtained from a best fit to Hugoniot data to 20 GPa. Below this pressure the degree of dissociation is negligible. The precise functional form is written as $\phi_{YR}(r)$ in Eq. (5) of Ref. 4.

## C. Metallic fluid

The properties of the monoatomic fluid phase in Eq. (2) are approximated by a metallic fluid equation of state. The expression for the free energy of the fluid is modeled after that of liquid metal perturbation theory. This model combines a density-dependent nearly-free-electron gas and a modified one-component plasma (OCP) ion-thermal energy. We write the Helmholtz free energy per two atoms as

$$F_{H-H} = 2[F^0_{H-H} + F_{EG}(V) + f_{LDA} + F_{OCP}(V,T) + \delta_e], \tag{6}$$

where $F^0_{H-H}$ is the ion translational free energy. $F_{EG}(V)$ is the density-dependent energy of positive ions in a bcc lattice immersed in a free-electron gas:

$$F_{EG} = [2.21/r_s^2 - 0.916/r_s - 0.88/(r_s + 7.8)$$
$$- 1.792/r_s] \quad Ry / ion. \tag{7}$$

The terms are, respectively, the kinetic, exchange, correlation (Wigner), and Madelung energies. $r_s = [3/(4\pi\rho)]^{1/3}$ is the hydrogen ion sphere radius and $\rho$ is the H atom density in the pure fluid. The third term in Eq. (6), $f_{LDA}$, is equivalent to the Hartree energy in the pseudopotential theory of metals which arises from the difference in energy between the pseudopotential and the pure Coulomb potential. In terms of electron-band theory it is the difference between the energy

of a free electron gas and an exact total-energy calculation. We required that $F_{EG} + f_{LDA}$ fit the total energy local density approximation (LDA) calculations of metallic hydrogen.[35] A good fit is given by

$$f_{LDA} = -0.113\,82 + 0.003\,554 r_s - 0.012\,707 r_s^2 \quad Ry/ion. \tag{8}$$

$f_{LDA}$ includes all the screening and band-structure effects omitted by the simple free-electron-gas model.

The last two terms in Eq. (6) are the thermal free energy of a one-component plasma and a correction ($\delta_e$) needed to precisely fit the reflected shock data. The OCP is a model in which positive ions are immersed in a constant density background of negatively charged fully degenerate electrons. Electron-ion screening and other nonideal effects are not included. This approximation is believed to be rigorous at extremely high densities. The thermal energy per ion of the OCP fluid has been determined by computer simulations and the Helmholtz free energy can be expressed by the functional form[34]

$$F_{OCP}/NkT = 4(b\Gamma^{1/4} - c/\Gamma^{1/4}) + (d)\ln\Gamma - e \tag{9}$$

where $\Gamma = (Ze)^2/r_s kT$, $b = 0.952\,80$, $c = 0.189\,07$, $d = -0.817\,73$, and $e = -2.59$. DeWitt and Rosenfeld[45] found that this functional form could be obtained from a variational hard-sphere calculation that included the virial entropy. Since then, it has been used to represent the equation of state for the OCP.

We find that by adjusting the value of $\delta_e$ to $-2.6$ that an excellent fit can be obtained to all the existing shock temperature and Hugoniot data. Since the shock data cover a relatively narrow range of $\Gamma = 33$–$45$, the approximation of $\delta_e$ as a constant can be viewed as justified over this regime. In terms of liquid metal theory, $\delta_e$ includes higher-order corrections due to electron-ion screening. The model presented here is the simplest and most transparent. It has the nice feature that it retains the analytic form of the OCP and allows for systematic improvements in the model. However, it appears that even improved models are unlikly to be accurate in so complicated a problem without introducing some fitting parameters. Even in the case of static or undissociated shock-compressed molecular hydrogen, an intermolecular potential has to be fitted to ensure an accurate representation of the equation of state. But most essential for this study is that the model provides an accurate equation of state for impedance matching the experimental data and for acquiring insight into the underlying physics.

## D. Mass action law

Minimization of $F$ with respect to $x$ leads to the well-known law of mass action for the equilibrium value of $x$:

$$x^2 = \frac{q}{4+q}, \tag{10}$$

where

$$q = \exp[-(F_{H-H} - F_{H_2} - D^0)/kT]. \tag{11}$$

Substituting Eqs. (4) and (6) into Eq. (11) leads to
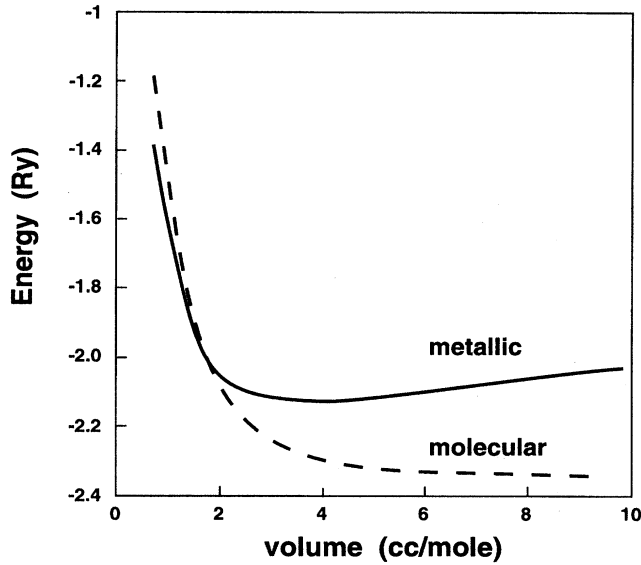
FIG. 5. Static lattice energy versus volume for molecular and metallic hydrogen at $T=0$ K. The energy of the isolated hydrogen atom ($-1$ Ry) is taken as the reference.

$$q = \exp\{-[(F^0_{H\text{-}H} - F^0_{H_2} - F^0_{H_2\text{int}})$$
$$+ (F_{EGOCP} - F_{H_2\,\text{conf}}) - D^0]/kT\}, \qquad (12)$$

where $F_{EGOCP} = F_{EG} + f_{LDA} + F_{OCP} + \delta_e$. The superscripted isolated particle free energies can be written in terms of atomic and molecular partition functions $Q$, leading to the expression

$$q = \left[ \frac{Q^0_H Q^0_H}{Q^0_{H_2} Q^0_{H_2\text{int}}} \exp(-D_e)/kT \right], \qquad (13)$$

where $D_e(V,T) = F_{EGOCP} - F_{H_2\text{conf}} - D^0$. $Q^0_H$ and $Q^0_{H_2}$ are translational partition functions and $Q^0_{H_2\text{int}}$ is the internal partition function for the vibrational and rotational degrees of freedom. Electron thermal excitation is negligible, but can be included. The exact expressions and standard values of the molecular parameters are cited in Hill.[36] The "law of mass action" is widely used for determining the fraction of molecular dissociation in gases and the ionization equilibria of plasmas. It has been rederived here in a more general fashion applicable to dense fluids. In the low-density limit the configurational free energy of the mixture is negligible and the expression reduces to the ideal gas limit. However, at high densities this is not the case and it is necessary to include the excess free energy of the interacting particles in the expression for $D_e$. Thus the model provides a thermodynamically self-consistent calculation of $D_e$ at high density which is the change in free energy required to dissociate a diatomic molecule. It is an effective-density and temperature-dependent dissociation energy.

$D_e(V,T)$ is the difference in energy between the metallic and molecular states; the total energies at 0 K of these states are plotted in Fig. 5. The molecular energies were calculated for a close-packed lattice using the pair potential previously
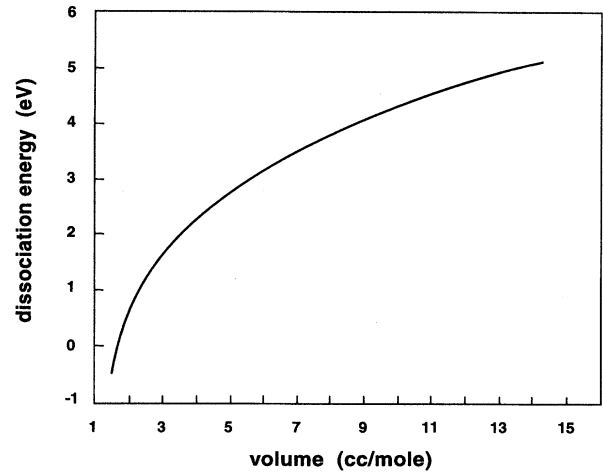


FIG. 6. Dissociation energy $D_e$ vs volume at $T=0$ K. $D_e$ is the difference in energy between the two curves in Fig. 5.

fit to shock data[4] and used here to calculate $F_{H_2\text{conf}}$. The crossing of the curves indicates that the molecular solid will undergo a transition to the metallic state. A calculation of the Gibbs energy for the two phases predicts a transition to a bcc metal above 5 Mbar in general agreement with prior calculations.[12] Plotted in Fig. 6 is $D_e(V,0)$, the difference in energy between the two structures at 0 K. $D_e(V,0)$ goes to zero near 1.5 cm$^3$/mol. At large volumes the predicted value of $D_e$ rises above the ideal gas value. However, at densities for which the calculated values of $D_e$ are too high, the shock temperatures are too low to cause any dissociation.

Physically, the existence of a density-dependent dissociation energy can be understood by comparing the dissociation of a molecule in an ideal gas to one at high density. In the gas phase an energy of 4.735 eV is required to break the interatomic bond and move the atoms to infinite separations. At high density some of the energy used to break the bond is returned when atoms recombine in a condensed system. Thus, there is an effective decrease in the energy required for dissociation, as described in Figs. 5 and 6.

Expressions for the pressure and energy are derived from the free energy and can be written as

$$P = (1-x)(kT/V + P_{H_2\text{conf}}) + x[2(kT/V) + P_{EGOCP}], \qquad (14)$$

$$E = (1-x)(K + U_{H_2\text{int}} + U_{H_2\text{conf}} + D^0) + x(2K + U_{EGOCP}), \qquad (15)$$

where $K = 3kT/2$ is the kinetic energy per particle. $U_{H_2\text{int}}$ is the energy of the molecular internal degrees of freedom.[4] $U_{H_2\text{conf}}$ and $U_{EGOCP}$ are the excess energies of the molecular hydrogen and electron gas-OCP fluids. $P_{H_2\text{conf}}$ and $P_{EGOCP}$ are the excess pressures. $P_{H_2\text{int}}$ does not appear in Eq. (14) because the molecular internal degrees of freedom have the ideal gas, density-independent values.
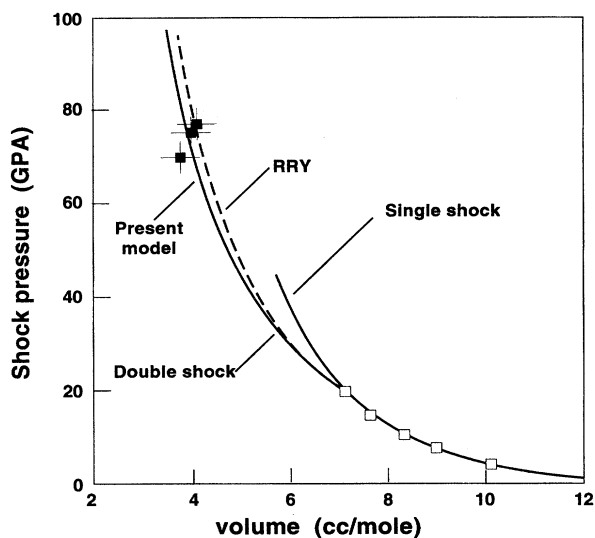
FIG. 7. Single- and double-shocked liquid deuterium Hugoniots. Experimental data from Ref. 1. The solid curve was calculated with the present model and the dashed curve with the model described in RRY (Ref. 4). The initial conditions are for the liquid at 1 bar and 20.3 K and reflected from 7.1 cm³/mol.

## IV. CALCULATIONS

The final $P,V,E$ state attained in a shock experiment is determined by the Hugoniot relations[23]

$$P - P_0 = \rho_0 u_s u_p,$$

$$V = V_0\left(1 - \frac{u_p}{u_s}\right), \qquad (16)$$

$$E - E_0 = (P + P_0)(V_0 - V)/2,$$

where $E$, $P$, and $V$ are the total energy, pressure, and volume. The initial density is $\rho_0 \equiv 1/V_0$, the velocity of shock propagation is $u_s$, and the material velocity behind the shock front is $u_p$. Subscripted (0) variables refer to initial conditions and unsubscripted to final states. The locus of $P$ and $V$ points satisfying Eq. (16) and originating from the same initial conditions is called the Hugoniot. In the case of reflected experiments the calculated final state is determined by impedance-matching[23] the reflected $P$ vs $u_p$ curve against that of the reflecting anvil which is also a window for these experiments. Table III contains a summary of the experimental and calculated shock temperatures for single- and double-shocked $D_2$ and for a single shock in $H_2$. The pressures and volumes for the double-shock states are calculated using the present model. The overall agreement between theory and experiment is excellent.

There have been several predictions of a band-gap closure in solid molecular hydrogen, the most recent by Chacham and Louie.[37] We introduced this effect into the model by allowing the first excited state in the electronic partition function [Eq. (13)] to decrease quadratically, as suggested by Chacham and Louie's results, going to zero at 2.5 cm³/mol (near 150 GPa). This leads to an additional lowering of the
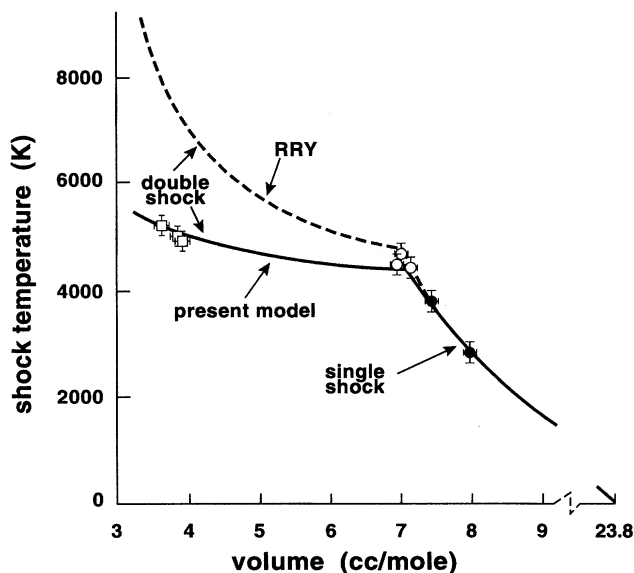


FIG. 8. Single- and double-shocked liquid deuterium temperatures vs volume. The solid curve was calculated with the present model and the dashed curve with RRY (Ref. 4). Circles indicate single-shock states; open circles and open squares indicated pairs of single-shock (circle) and double-shock (open squares) states. The initial conditions are for the liquid at 1 bar and 20.3 K and reflected from 7.1 cm³/mol on the single-shock Hugoniot.

shock temperatures by about 100 K near 5200 K and is negligible for the remaining lower-density data. At higher temperatures and densities the increasing monatomic concentration makes the concept of a molecular band gap in the fluid questionable. Given its speculative nature and small magnitude we chose to neglect this effect.

A nice illustration of the important role temperature measurements play in constraining models is shown by the Hugoniot and shock temperature data plotted in Figs. 7 and 8, respectively. The first- and second-shock Hugoniot measurements in Fig. 7 are from the work of Nellis et al.[1] and the temperature measurements in Fig. 8 are those reported here. The calculated Hugoniots in both figures are from the present theory and RRY.[4] RRY used the same $H_2$-$H_2$ potential. It can be shown[38] that their model is equivalent to approximating the $H_2$-$H$ potential to be 1/2 of the $H_2$-$H_2$ potential and the H-H potential to be 1/4 of the $H_2$-$H_2$ potential. The dissociation energy was fixed at the ideal gas value. Note that while both sets of calculations are in agreement with the single- and double-shock Hugoniots in Fig. 7 and the single-shock temperatures in Fig. 8, the calculated double-shock temperatures differ by up to 40%. The reason for the apparent agreement of the pressures can be explained by the fact that although the enhanced dissociation of the present model leads to a large drop in thermal pressure per particle, it is partially offset by a rise due to the increased number of particles. Calculated single-shock temperatures below 20 GPa are in good agreement with experiment for both theories because the dissociation is small or negligible, as seen in Table III. We return to the importance of temperature as a theoretical constraint in the next section.

## V. DISCUSSION

From a theoretical point of view, the study of hydrogen offers a special opportunity to clarify and choose the important approximations necessary for a successful model. An inspection of the total energy curves for the metallic and molecular solid phases shown in Fig. 5 provides insight into the interatomic force. The total energy of the molecular form has a minimum at $P = 0$ near 24 cm$^3$/mol (not shown). Since the forces between closed-shell molecules under pressure are mainly repulsive, the total energy rises continuously with increasing density. In contrast the energy of the metallic form reaches a minimum near 4 cm$^3$/mol $H_2$ in the immediate region of the experimental reflected shock data. The energies of the two curves cross near 1.5 cm$^3$/mol $H_2$. These are theoretically well-established features of the hydrogen equation of state. They show that the effective interactions between atoms in the monatomic state are much less repulsive than in the molecular and as a result the dissociation energy, which is the difference between the two curves, decreases monotonically with increasing density and reaches zero at the curve crossing. In terms of the fluid equation of state, the lowering of $D_e$ leads to enhanced dissociation which acts as a thermal sink that lowers the shock temperature. Thus it is the softer forces of the monatomic system which leads to the lowering of the dissociation energy that is ultimately responsible for the lower temperatures.

In two papers, Saumon and Chabrier[39,31] have developed models to calculate the equation of state of neutral and partially ionized hydrogen for modeling the Jovian planets. Their work was completed prior to our present temperature measurements and hence they were limited to the available Hugoniot measurements[1] to test their predictions. Their model differs sufficiently from ours to make an intercomparison highly informative. To make a direct connection to our own model we express their free energy in terms analogous to those in Eq. (2):

$$F = (1-x)^2 F_{H_2} + 2x(1-x)F_{H_2-H_a} + x^2 F_{H_a-H_a} - TS_{mix}$$
$$+ (1-x)D^0. \tag{17}$$

The terms refer to the $H_2$-$H_2$, $H_2$-$H_a$, and $H_a$-$H_a$ interactions. The principal formal difference with Eq. (2) is the inclusion of $H_2$-$H_a$ interactions. Here the terms $H_2$-$H_a$ and $H_a$-$H_a$ are used to designate true molecular-atomic and atomic-atomic interactions and should not be confused with the $H_2$-H and H-H terms in previous equations. The $H_2$-$H_2$ potential they use is the same we use here. Their $H_2$-$H_a$ and $H_a$-$H_a$ potentials were obtained from a theoretical model for isolated pairs of particles. These potentials exhibit an energy minimum near 3 Å and rise exponentially with decreasing interatomic separation. Their Hugoniot falls very close to the curve of RRY plotted in Fig. 7. Figure 9 plots two sets of their calculated temperatures reshocked from a volume of 7.1 cm$^3$/mol and those from the present study. The predicted temperatures are considerably higher than the values reported here by almost 2000 K at the highest experimental densities, or nearly 40%. This leads us to conclude that their $H_2$-H and H-H interactions are too repulsive. In fact, the higher temperature obtained in their more recent results[31] is
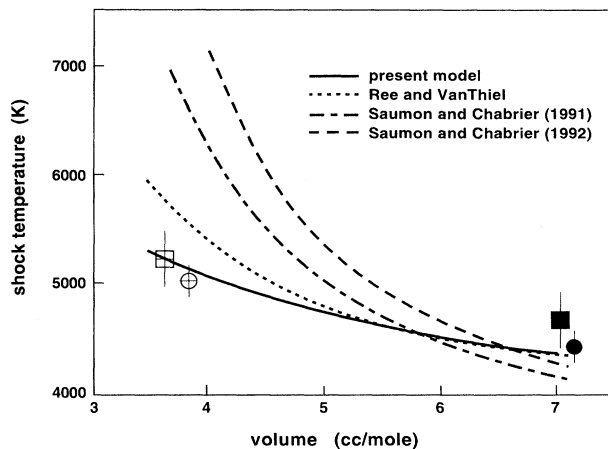


FIG. 9. Reflected shock temperature measurements and theory. Squares refer to experiment $D_2$ No. 1 and circles to $D_2$ No. 2; solid points are the first-shock states and open symbols indicate the second-shock states. In the calculations, the second-shock state is reflected from 7.1 cm$^3$/mol on the single-shock Hugoniot. The solid curve is the present model described in the text. Those calculations are compared with those from Saumon and Chabrier (Refs. 39,31) and of van Thiel and Ree (Refs. 40,42).

the result of arbitrarily stiffening the potentials in order to force a complete dissociation at metal-like densities.

To directly verify our conclusions regarding the need for a soft equation of state for the dissociated fluid, Hugoniot calculations were made by van Thiel[40] with the CHEQ model,[41] which is similar to that of Saumon and Chabrier. van Theil used an $H_2$-$H_2$ potential fitted to the shock data[1] and an exponential-6 $H_a$-$H_a$ potential suggested by Ree[42] for which $\alpha = 13.0$, $r^* = 1.4$ Å, and $\epsilon/k = 20$ K. This $H_a$-$H_a$ potential predicts a minimum energy for a close-packed monatomic hydrogen solid near 2.4 cm$^3$/mol $H_2$, very close to the LDA results of Barbee in Fig. 5. It favors dissociation at high pressure and at low temperature the dissociation is a first-order phase change. The H-$H_2$ parameters were determined using the Berthelot mixing rules, which composition averages the $H_2$-$H_2$ and $H_a$-$H_a$ values of $r^*$ and $\epsilon/k$. The resulting Hugoniot temperatures, included in Fig. 8, show a very dramatic drop from those predicted by Saumon and Chabrier. The results included in Fig. 9 show very clearly the need for a soft $H_a$-$H_a$ interaction and the great importance of shock temperature measurements for constraining theoretical models and for determining the essential features of the effective potentials.

The CHEQ model provides us with an opportunity to test the linear approximation of Eq. (2) near the highest experimental reshock density where dissociation is greatest. Ideal mixing predicts that the total pressure is given by

$$P = (1-x)P_{H_2}(V,T) + xP_{H_a-H_a}(V,T), \tag{18}$$

where $P_{H_a-H_a}$ is the total pressure of two atoms in a volume $V$. $P_{H_2}$ and $P_{H_a-H_a}$ were calculated at $V = 3.68$ cm$^3$/mol and $T = 5780$ K along the Hugoniot for which the CHEQ pressure was 82.5 GPa. Ree's $H_a$-$H_a$ potential was used.[42] Using the CHEQ model's calculated value of $x$ (0.268), the linear

approximation predicts a pressure of 84.1 GPa. This is an error of only 1.9%, well within the experimental uncertainty.

Hydrogen and nitrogen are both diatomic solids in which the insulator-metal transition is of considerable interest. A brief comparison of the two is worthy of a short digression because of the insight it may provide. Total-energy calculations for solid molecular nitrogen and several higher-energy structures[43] provide a picture of total-energy curves similar to those calculated for solid deuterium in which the energies cross at a high pressure. Single-shock temperatures were reported for liquid nitrogen that were lowered by the presence of dissociation and second-shock temperatures were recorded near 7000 K and 70 GPa that were lower than the first-shock temperature.[5,6] In other words cooling was observed on reshocking. Although cooling has not been observed on reshocking deuterium, a greatly lowered final temperature was obtained. A model similar to the present one, which included a dissociation energy that decreased with increasing density, was successful in interpreting the nitrogen experiments.[38,44] Thus we believe that the similar behavior of deuterium and nitrogen suggests a general pattern for closed-shell diatomic systems.

The present model takes a phenomenological approach. It defines a free-energy function in which a single parameter $\delta_e$ is adjusted to fit all the available shock data and it extrapolates correctly to high and low density. We believe it provides a reasonable prediction of the second-shock pressure and density. It does not purport to be a universal theory of dense hydrogen. But it does take a unique approach to a very difficult problem and provides a basis for further development.

## ACKNOWLEDGMENTS

[1] W.J. Nellis, A.C. Mitchell, M. van Thiel, G.J. Devine, R.J. Trainor, and N. Brown, J. Chem. Phys. 79, 1480 (1983).
[2] M. van Thiel, L.B. Hord, W.H. Gust, A.C. Mitchell, M. D'Addario, K. Boutwell, E. Wilbarger, and B. Barrett, Phys. Earth Planet. Inter. 9, 57 (1974).
[3] W.J. Nellis, A.C. Mitchell, P.C. McCandless, D.J. Erskine, and S.T. Weir, Phys. Rev. Lett. 68, 2937 (1992).
[4] M. Ross, F.H. Ree, and D.A. Young, J. Chem. Phys. 79, 1487 (1983).
[5] H.B. Radousky, W.J. Nellis, M. Ross, D.C. Hamilton, and A.C. Mitchell, Phys. Rev. Lett 57, 2419 (1986).
[6] W.J. Nellis, H.B. Radousky, D.C. Hamilton, A.C. Mitchell, N.C. Holmes, K.C. Christianson, and M. van Thiel, J. Chem. Phys. 94, 2244 (1991).
[7] H.B. Radousky, M. Ross, A.C. Mitchell, and W.J. Nellis, Phys. Rev. B 31, 1457 (1985).
[8] H.B. Radousky and M. Ross, Phys. Lett. A 129, 43 (1988).
[9] N.C. Holmes, Rev. Sci. Instrum. 66, 2615 (1995).
[10] C-S. Yoo, N.C. Holmes, M. Ross, D.J. Webb, and C. Pike, Phys. Rev. Lett. 70, 393 (1993).
[11] E. Wigner and H.B. Huntington, J. Chem. Phys. 3, 764 (1935).
[12] T.W. Barbee and M.L. Cohen, Phys. Rev. B 44, 11563 (1991).
[13] V. Natoli, R.M. Martin, and D. Ceperley, Phys. Rev. Lett. 70, 1952 (1993).
[14] N.W. Ashcroft, Phys. Rev. B 41, 10963 (1990).
[15] E. Kaxiras, J. Broughton, and R.J. Hemley, Phys. Rev. Lett. 67, 1138 (1991).
[16] M.P. Surh, T.W. Barbee, and C. Mailhiot, Phys. Rev. Lett. 70, 4090 (1993).
[17] H.E. Lorenzana, I.F. Silvera, and K.A. Goettel, Phys. Rev. Lett. 65, 1901 (1990).
[18] R.J. Hemley and H.K. Mao, Science 249, 391 (1990).
[19] L. Cui, N.H. Chen, and I.F. Silvera, Phys. Rev. Lett. 72, 3048 (1994).
[20] H.K. Mao and R.J Hemley, Rev. Mod. Phys. 66, 671 (1994).
[21] A. H. Jones, W. M. Isbell, and C. J. Maiden, J. Appl. Phys. 37, 3493 (1966).
[22] A. C. Mitchell and W. J. Nellis, Rev. Sci. Instrum. 52, 347 (1981).
[23] Ya. B. Zel'dovich and Yu. P. Raizer, Physics of Shock Waves and High-Temperature Hydrodynamic Phenomena (Academic, New York, 1967), Vol II, p. 726.
[24] W.J. Nellis, F.H. Ree, M. van Thiel, and A. C. Mitchell, J. Chem. Phys. 75, 3055 (1981).
[25] A.C. Mitchell and W.J. Nellis, J. Appl. Phys. 52, 3363 (1981).
[26] N.C. Holmes, J.A. Moriarty, G.R. Gathers, and W.J. Nellis, J. Appl. Phys. 66, 2962 (1989).
[27] Los Alamos Shock Hugoniot Data, compiled by S.P. Marsh (University of California Press, Berkeley, 1980).
[28] D.J. Erskine, in High-Pressure Science and Technology–1993, edited by S.C. Schmidt, J.W. Shaner, G.A. Samara, and M. Ross, AIP Conf. Proc. No. 309 (AIP, New York, 1994), pp. 141–143.
[29] W.H. Press, B.P. Flannery, S.A. Teukolsky, and W.T. Vetterling, Numerical Recipes in C, The Art of Scientific Computing (Cambridge University Press, Cambridge, England, 1988).
[30] K.-I. Kondo, in High-Pressure Science and Technology-1993, edited by S.C. Schmidt, J.W. Shaner, G.A. Samara, and M. Ross, AIP Conf. Proc. No. 309 (AIP, New York, 1994), pp. 1555–1558.
[31] D. Saumon and G. Chabrier, Phys. Rev. A 46, 2084 (1992).
[32] D. Hohl, V. Natoli, D.M. Ceperley, and R.M. Martin, Phys. Rev. Lett. 71, 541 (1993).

[33] E.A. Guggenheim, *Mixtures* (Oxford University Press, Oxford, 1952).

[34] W.L. Slattery, G.D. Doolen, and H.E. DeWitt, Phys. Rev. A **21**, 2087 (1980). The values of the coefficients used in this work were recommended by DeWitt and differ slightly from those in the reference.

[35] T.W. Barbee III (private communication). See Ref. 12 for details.

[36] T.L. Hill, *An Introduction to Statistical Thermodynamics* (Addison-Wesley, Reading, MA, 1960).

[37] H. Chacham and S.G .Louie, Phys. Rev. Lett. **66**, 64 (1991).

[38] M. Ross, J. Chem. Phys. **86**, 7110 (1987).

[39] D. Saumon and G. Chabrier, Phys. Rev. A **44**, 5122 (1991).

[40] M. van Thiel (private communication).

[41] F.H. Ree, J. Chem. Phys. **81**, 1251 (1984).

[42] F.H. Ree, in *Shock Waves in Condensed Matter—1987*, edited by S.C. Schmidt and N.C. Holmes (Elsevier, New York, 1988), p. 125.

[43] C. Mailhiot, L.H. Yang, and A.K. McMahan, Phys. Rev. B **46**, 14419 (1992).

[44] H. Lorenzana (unpublished).

[45] H.E. DeWitt and Y. Rosenfeld, Phys. Lett. **75A**, 79 (1979).